Influence of Concentration Gradients on Electroconvection at a Cation-Exchange Membrane Surface

*Qingpu Wang[a], Jaehun Chun[b], and Chinmayee V. Subban[a,c]**

[a] Energy and Environment Directorate, Pacific Northwest National Laboratory, Seattle, WA 98109, USA

[b] Physical and Computational Sciences Directorate, Pacific Northwest National Laboratory, Richland, WA 99354, USA

[c] Department of Materials Science and Engineering, University of Washington, Seattle, WA 98195, USA

*Email: chinmayee.subban@pnnl.gov

ABSTRACT

Membrane-based systems such as electrodialysis play an important role in desalination and industrial separation processes. Electrodialysis uses alternating anion- and cation-exchange membranes with a perpendicular electric field to generate concentrate and diluate streams from a feed solution. It is known that under overlimiting current conditions, reduced charge and mass transfer at the membrane interface leads to regions of high ion-depletion generating instability and vortices referred to as electroconvection. While electroconvective mixing is known to directly impact the separation efficiency of electrodialysis, the influence of ion concentration gradients across the membrane experienced in a functional electrodialysis system is not known. Here, we report the influence of ion concentration gradients across a cation exchange membrane (Nafion) both aligned and opposed to the applied electric field. Experiments were conducted by co-flowing NaCl solutions of different concentrations (0.1 to 100 mM) on each side of the membrane, and electroconvection was visualized with a fluorescence dye (Rhodamine 6G). We obtained concentration profiles from fluorescence image data and systematically measured the thickness of the depletion boundary layer d_{BL} under different conditions. We found smaller d_{BL} values at a higher flow rate both with and without concentration gradients. Our results show that electroconvection is enhanced when the electric field is opposite to the direction of the concentration gradient.

INTRODUCTION

All human activities from agriculture to industrial manufacturing require freshwater. Due to a combination of climate change and population growth, reliable access to freshwater is becoming increasingly scarce.[1] Building a climate-resilient, energy-efficient water infrastructure that can supply the necessary quality and quantity of freshwater will need to rely on diverse and non-traditional water sources,[2] which includes desalination of brackish and seawater sources and the treatment and reuse of industrial, agricultural, and municipal wastewater streams. To enable such next-generation, distributed, and decentralized freshwater production, electric-field driven treatment processes powered by renewable energy sources are particularly attractive. Electrodialysis (ED) is one such promising technology that is commercially available and is currently utilized for various industrial processing and water treatment applications.[3] An ED unit consists of alternating cation-exchange membrane (CEM) and anion-exchange membranes (AEM) sandwiched between two electrodes, with feedwater flowing parallel to the membranes. When a voltage is applied across the electrodes (perpendicular to feedwater flow), alternating streams of concentrate and diluate water streams are generated due a combination of permselectivity of the AEMs and CEMs and the transport of co-ions and counter ions towards oppositely charged electrodes.

ED has been extensively studied both theoretically and experimentally towards achieving optimum performance and maximum energy efficiency. Significant research has been focused on improving membrane performance and lifetime (minimize scaling and fouling),[4] or reducing cost of system components,[5] but overall process efficiency can also be improved by developing a better understanding of ion-transport in these systems. One such ion-transport phenomenon of importance is electroconvection. Electroconvection occurs with increasing applied voltages where limiting charge and mass transfer at the membrane-electrolyte interface leads to regions of high ion-depletion, and the instability generates vortices. Such hydrodynamic instabilities, referred to as electroconvection can improve ion transport and mixing at the membrane interface. [6-10]

First theoretically developed by Rubinstein *et al.,*[11-13] electroconvection is experimentally observed as vortices in the ion depletion layer at membrane/solution interface under overlimiting currents.[9] The physical origin of electroconvection has been attributed to electro-osmosis and the formation of the extended space charge region at ion-selective surfaces.[14,15] A variety of setups with different membranes,[16-20] resin contents,[21] and electrodes/electrolyte chemistries[22-28] have been used in experimental studies to-date. The choice of electrode/electrolyte determines the electrochemical reactions (e.g., water splitting, electrodeposition) occurring in the system which may directly influence onset and/or nature of electroconvection. Typically, for vortex visualization, the studies spike electrolyte solutions either with tracer particles for flow profiles and/or fluorescent molecules for concentration profiles.[29] More recently, studies have also focused on understanding the influence of physical adaptation of electroconvection by introducing geometric patterns on the surface of the membrane[30,31] and by adding reinforcing structures in the membrane.[32] Although most of the early studies used a stagnant electrolyte reservoir,[33] Kwak *et al.* introduced the use of microfluidic devices to study electroconvection under fluid flow.[24,34,35]

Irrespective of stagnant reservoir or fluid flow configuration, all previous electroconvection studies have focused on a single electrolyte solution in contact with the IEM and have not investigated the influence of concentration gradients across an IEM. Given that concentration/salinity gradient plays a vital role in both ED and reverse ED,[36,37] we created such gradient by co-flowing two electrolyte solutions in channels separated by a cation-exchange membrane. Each channel also contains a titanium (Ti) electrode for electrical contact. These two channels mimic the neighboring channels with concentrate and diluate in an electrodialysis unit. The device can be easily altered to include a reference electrode for three-electrode electrochemical analysis, and the system design allows real-time observations of the membrane surface with co-flowing solutions on either side. Using this configuration, we report the influence of concentration gradients across the IEMs when the direction of the electric field is aligned with or opposite to the direction of the concentration gradient.

EXPERIMENTAL

Chemicals. Sodium chloride (NaCl, GR ACS grade, SX0420-3, Sigma-Aldrich) and rhodamine 6G (R6G, $C_{28}H_{31}ClN_2O_3$, 99%, AC419010250, Fisher Scientific) were used as received. All solutions were prepared with ultrapure water filtered by a Milli-Q IQ 7000 water purification system (resistivity 18.2 MΩ·cm).

Construction of the Microfluidic Device. We designed and constructed a microfluidic device with integrated electrodes and ion-exchange membrane. The construction method was adapted from our previously reported technique.[38] Figure 1a shows the exploded view of the microfluidic device that mainly contains a cut parafilm membrane sandwiched between two polycarbonate plates (thickness 1.6 mm each). Four small holes (diameter 1.6 mm) were drilled onto the top plate along the two shorter edges, and four barb fittings (inner diameter 1.6 mm, NResearch Inc., FITM 331) were glued onto the holes as the inlets and outlets. Additionally, four larger holes (diameter 3.0 mm) were created in the middle on both plates and the parafilm to position the screws and nuts for fastening. The parafilm membrane was cut using an electrical cutting machine (Silhouette Portrait 3) using a custom design consisting of a double Y-shape as the main fluid channel and a thin rectangular shape in the middle that extended beyond the stem of the Y-shape to match the outline of the Nafion membrane (N115, thickness 0.13 mm). The rectangular shape perpendicular to the flow channel was cut to accommodate the electrodes. In this study, we used metallic titanium (Ti) for both the working and the counter electrodes. The Ti sheet (thickness 0.13 mm) was manually cut into rectangular strips (5.9 mm × 25 mm) and then folded into a Z shape to allow device operation on a narrow microscope stage. Thin copper wires (diameter 0.13mm) were wrapped around the Ti electrodes to electrically connect the device to the potentiostat. The Nafion membrane was cut into rectangular strips (0.9 mm × 18 mm) using the same silhouette cutting machine and soaked in 0.5 M NaCl overnight. Before use, the soaked Nafion strips were rinsed thoroughly with DI water. All the components were placed in the order shown in the deconstructed view in Figure 1a, and the assembled device was heated on a hot plate (VWR) at low heat for 3 min until the parafilm slightly melted and became transparent. After cooling down to room temperature, the parafilm seals the device to avoid potential leakage (Figures 1b, c). We note that to ensure minimal leaking, the Nafion membrane, Ti electrodes, and the parafilm were all of the same thickness (0.13 mm). A top view of these parts is shown in Figure 1d.

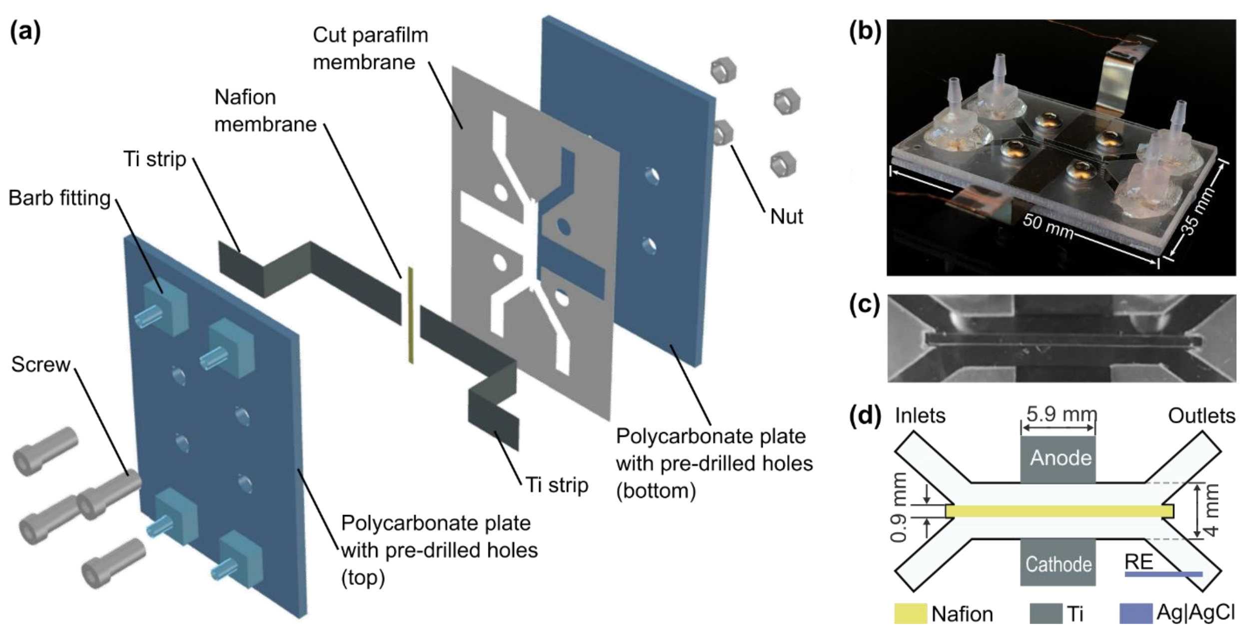

Figure 1. (a) Deconstructed view showing the components of the microfluidic device. (b) Photograph of the assembled microfluidic device. Thin Ti sheets were used as the electrodes on

each side. (c) Magnified view showing a Nafion membrane placed horizontally in the middle to separate the flow channels for the two salt solutions during the experiment. (d) Schematic highlighting the different system components.

Preparation of Electrolyte Solutions. The NaCl solutions of different concentrations from 0.1 mM to 100 mM were used as the co-flow electrolytes. All solutions also contained 10 μM R6G for visualizing the concentration profiles to measure the thickness of the depletion boundary layer d_{BL}. The choice of R6G and its concentration in our study was determined based on previous studies on tracing salt concentrations using optical fluorescence techniques.[24] Note that d_{BL} can largely reflect the size of electroconvection vortex zone d_{EC} and that the difference is the diffusive boundary layer δ ($\delta = d_{BL} - d_{EC}$).[34] d_{EC} can be measured experimentally using fluorescent tracer particles,[25,30] while δ is much smaller than d_{EC} and can be calculated for different flow conditions.[39,40]

Electroconvection Experiments. The schematic diagram in Figure 2a shows the overall experimental setup. The microfluidic device was attached to the stage of a fluorescence microscope (Thermo Fisher Scientific, EVOS FL Auto) using two bulldog clips. Two syringes containing NaCl solutions (c_A and c_B) were connected to the inlets to the device, where c_A and c_B represent the salt concentrations in the lower and upper channels (see Figure 1c), respectively, and can generate a positive, zero, or negative concentration gradient from channel A to channel B for $c_A < c_B$, $c_A = c_B$, and $c_A > c_B$, respectively. The solutions were injected using two identical syringe pumps (New Era, NE-300) at a constant flow rate between 0 and 1.0 mL/h.

The electrolyte solutions were continuously pumped into the microfluidic channels for 10 min before each experiment to eliminate any air bubbles. A short plastic tubing (inner diameter 1.6 mm, length 15 cm) was directed from the outlet on the side of channel B to a 2 mL centrifuge tube, where a miniature Ag|AgCl reference electrode was inserted. Then, the Ti and reference electrodes were connected to the potentiostat (BioLogic SP-200) for applying a voltage and measuring the current response. In a typical experiment, the applied field was from channel A to channel B and for experiments to study influence of field reversal, the polarity was switched (dashed arrow in Figure 2b), and the reference electrode was also switched from channel A to channel B for consistency.

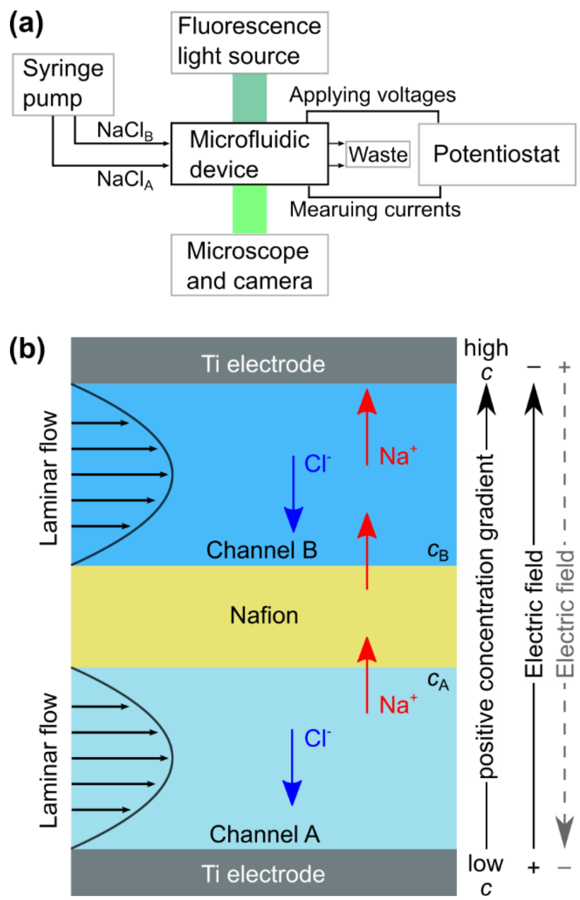

Figure 2. Schematics of (a) the entire experimental setup and (b) the interfaces across the Nafion membrane. The setup can control the concentration gradient and the direction of the electric field. In this illustration, the concentration gradient from channel A to channel B is positive, with salt concentrations $c_A < c_B$. The direction of the electric field can be reversed by simply switching the polarity as indicated by the dashed gray line.

The maximum Reynolds number Re for our system was calculated to be 0.34 using the equation $Re = \frac{QD_\mathrm{H}}{\nu A}$ where ν and D_H represent the kinematic viscosity of water and the hydraulic diameter of the channel, respectively. The cross-sectional area A varied slightly from different devices due to variabilities in the relative position of the Nafion membrane and electrodes. The small Re suggests that flows are under a laminar flow regime which has been established as ideal for the study of electrodialysis even in compartments at larger scales.[41]

Device Operation and Microscopic Image Data Collection. We mainly used two electrochemical techniques for our characterizing electroconvection in our system, linear sweep voltammetry (LSV) and chronoamperometry (CA). For LSV, the voltage was set to increase from 0 to 10 V at a constant sweep rate of 100 mV/s based on conditions reported in a previous electroconvection study.[26] For CA, constant voltages were hold for 20-120 s. For visualizing the concentration profiles, we used a GFP mode of the fluorescence microscope with excitation and emission maxima near 482 and 524 nm. In a typical experiment, we started to collect image data simultaneously with the potentiostat program. The data acquisition included the collection of time-lapse images at four-second intervals and screen recording at 15 frames per second. These fluorescence image and video data were analyzed using in-house scripts in MATLAB (MathWorks, R2020b). Note that the view window was smaller than the total channel width (4 mm) and centered around the middle point of the 18-mm-long membrane strip (Figure S1 in the Supporting Information).

RESULTS AND DISCUSSION

Firstly, we tested the workable voltage range of our microfluidic system using the LSV technique. Figure 3a shows a representative current-voltage plot during our experiment as the applied voltage increased at a constant rate of 100 mV/s from 0 to 9 V. Three characteristic regimes of the underlimiting, limiting, and overlimiting current were observed.[9] In this experiment, the NaCl concentrations in the two channels were $c_A = 1$ mM and $c_B = 10$ mM, creating a positive concentration gradient from channel A to channel B ($\Delta c = c_B - c_A > 0$ where diffusion occurred in the opposite direction of Δc, i.e., from B to A), and the applied electric field was aligned with this gradient. Up to 1.8 V, there was no measurable current, indicating an induction period during which the field-driven ion transport through the Nafion membrane had to overcome the opposing concentration gradient. That is, the concentration field is very slightly perturbed from the equilibrium distribution. Note that the channel widths (about 1.6 mm) in the device are significantly larger than those in electrodialysis, where the membranes are separated by just a thin spacer layer, which could also contribute to the observed slow current response. As the voltage increased from 1.8 to 3.0 V, we observed a linear relationship between the current and voltage, indicating sustained ion transport across the membrane. However, when the applied voltage reached around 3.0-4.5 V, the current values stayed nearly constant with increasing voltages, suggesting a local ion depletion and resultant concentration polarization near the Nafion membrane surface. The nearly constant current measured here indicates a quasi-equilibrium state established by a counteract of the local electromigration and concentration-gradient-induced diffusion. At the voltages over 4.5 V, the current increased at a higher rate than the limiting regime with relatively large noise in the current data. Such increase in current was mainly due to enhanced ion transport caused by electroconvection. The relatively large noise was partially due to gas evolution from electrochemical side reactions (e.g., water splitting, chlorine evolution) which are common for systems using aqueous chloride eletrolytes.[24,42] The concentration profiles at the membrane-electrolyte interface and the possible mechanism of the three regimes have been previously reported and thoroughly described in both theoretical and experimental studies.[33,35,43-45]

Concurrent with the LSV measurements, we also recorded the ion transport activity in the microfluidic channel using a fluorescence microscope. These fluorescence image data can be translated into local ion concentration profiles. The frames in Figure 3b were cropped to show the area close to the Nafion membrane in channel A. We also color-coded the images based on relative changes in fluorescence intensity. This process was performed by computing the difference in image intensity between the frame at $t = 0$ and each consecutive frame using MATLAB. The red, blue, and black pixels represent positions with large, small, and no changes in fluorescence intensity, respectively. And a larger intensity change means a stronger depletion of cations in that area, since R6G is a cationic fluorescent dye. This procedure yielded pronounced color profiles and allowed us to clearly visualize and define the depletion boundary layer (Figure 3c), so all electroconvection images presented in the remainder of this study were processed in the same way. We note that the d_{BL} value was measured as the maximum thickness of the ion depletion layer in each condition (i.e., a maximum vortex size associated with electroconvection) that occurred at the highest currents. At $t = 36$ s, we observed a continuous dark blue band at the membrane surface (Figure 3b), suggesting the onset of changes in fluorescence image intensities and concentration polarization. With increasing voltages overtime, the dark blue band became light blue ($t = 52$ s) meaning a large change in image intensity (and ion depletion). The continuous band subsequently evolved into discrete asymmetric semicircular vortices. The size of these vortex zones showed an increasing trend along the flow direction in the beginning and became approximately uniform at later stages, analogous to a boundary layer for flows near a solid surface. These shapes also grew in the direction against the direction of the electric field and perpendicular to the flow direction, which is in agreement with previously reported characteristics of electroconvective vortices under shear flow.[34]

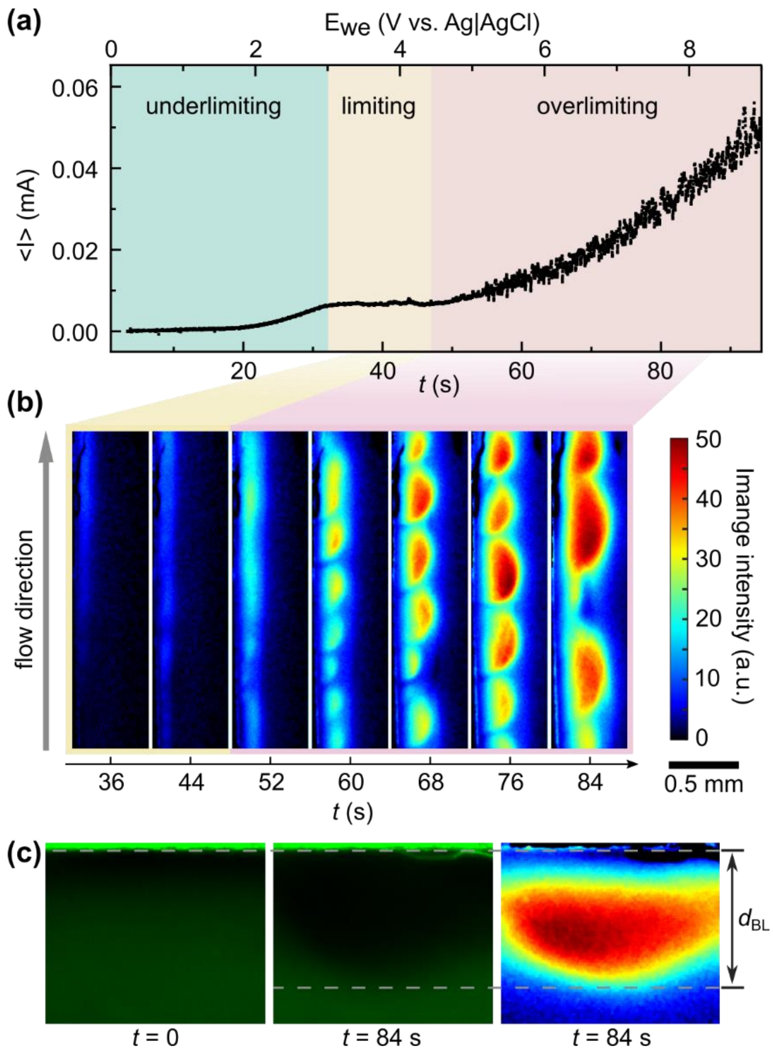

Figure 3. (a) Representative current-voltage curve during the LSV experiment. (b) Consecutive snapshots showing the temporal evolution of the electroconvection with a small concentration gradient across the Nafion membrane. Each frame shows the difference in image intensity of the current frame and the initial frame at $t = 0$. The black pixels indicate no intensity changes in the fluorescence signal, while the red pixels represent large intensity changes. (c) Comparison of the unprocessed with the false-colored images and the definition of d_{BL}. The top dashed line marks the border of the Nafion membrane. Experimental condition: $c_A = 1$ mM, $c_B = 10$ mM, $Q = 0.2$ mL/h.

Our microfluidic system allows us to simultaneously flow electrolyte solutions of different concentrations next to the Nafion membrane and to control the direction of the applied electric field. To qualitatively evaluate the influence of the concentration gradients, we performed two groups of experiments one with a negative concentration gradient ($c_A > c_B$, $\Delta c < 0$) and the other with positive concentration gradient ($c_A < c_B$, $\Delta c > 0$) across the Nafion membrane. In each case, current measurements were obtained with the applied electric field either aligned with or opposed to the direction of concentration gradient. The results are summarized in Figure 4 with the blue and red colors in a, c representing the aligned and opposite directions, respectively. For $c_B = 0.1$ mM, the differences in current were relatively small with a maximum of $\Delta I = 0.005$ mA (Figure 4a). For $c_B = 10$ mM, the maximum current, when opposed, was nearly ten times higher than when aligned (Figure 4c). In both cases, opposing concentration gradient and the electric fields yielded larger currents due to enhanced ion transport by electromigration.

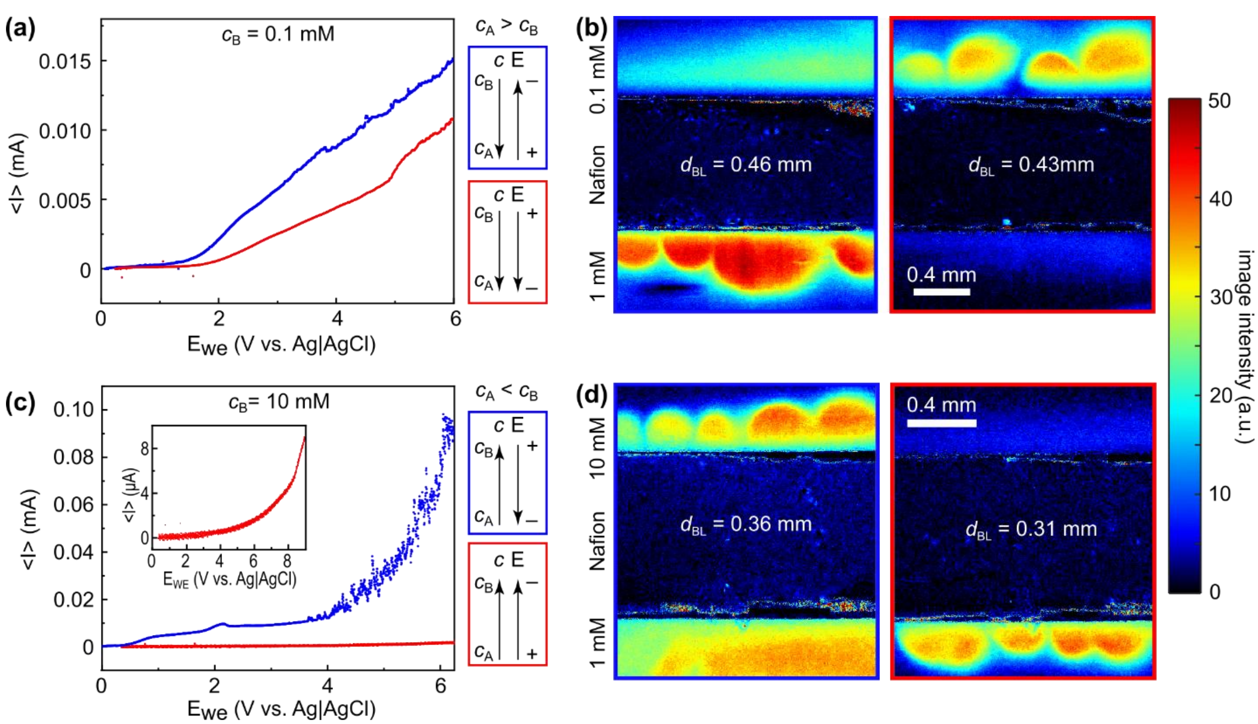

Figure 4. (a,c) Current-voltage plots when the direction of the electric field is opposite to (blue) or aligned (red) with the concentration gradient. (b, d) False-colored images showing largest d_{BL} values under each condition. The inset in (c) is the plot of the red curve with its complete range. Experimental conditions: c_B = 0.1 mM (a, b), c_B = 10 mM (c, d); c_A = 1 mM and Q = 0.2 mL/h for all.

False-colored images in Figures 4b,d show the field of view centered around the Nafion membrane between the two different concentration solutions (also see Movie S1-4 in the Supporting Information). Electroconvection was observed on either side of the Nafion membrane, determined by the direction of the applied electric field (Figure 4b,d). For both cases ($c_A > c_B$ and $c_A < c_B$), the measured currents and d_{BL} values were larger when the directions of the concentration gradient and the electric field were opposed. The increase in d_{BL} indicates enhanced electroconvection that also contributed to larger current fluctuations in the overlimiting regime, which is in agreement with the electrokinetic model predictions that enhanced electroconvection could appear at a homogeneous flat membrane surface.[39] Electroconvection was observed in the high concentration channel when the direction of the electric field was opposed to the direction of concentration gradient, and in the low concertation channel when aligned. Our results show that diffusion and electromigration contribute synergistically to the ion depletion and electroconvection at the Nafion membrane surface. Note that the intensity changes on the opposite side of the electroconvection channel in Figures 4b,d were likely artifacts of absorption and desorption of R6G on the Nafion membrane and could be potentially avoided by longer resetting times between measurements.

In the absence of concentration gradients ($c_A = c_B$), the largest d_{BL} value was obtained at 0.1 mM. We found that the d_{BL} value decreased with increasing concentrations at a constant flow rate of

0.2 mL/h (Figure 5a). These results suggest that a higher conductivity of the electrolyte could hinder electroconvection since a larger number of ions would need to be transported to achieve the same degree of local ion-depletion. To investigate the effect of concentration gradient, we systematically varied the NaCl concentration in the channel B, c_B, while keeping a constant concentration in the channel A, $c_A = 1$ mM. Note that here we held the direction of the electric field constant (A → B) and did not reverse polarity. We found that the d_{BL} value decreased slightly with increasing c_B at a constant flow rate of 0.2 mL/h (Figure 5b). For $c_B = 0.1$ mM, this condition generates a concentration gradient with its direction ($c_A > c_B$) aligned to the direction of the electric field. For $c_B = 10$ and 100 mM, the concentration gradient was aligned with the direction of the electric field. These trends in d_{BL} from changing concentrations are in agreement with our results obtained by switching the direction of the electric field while holding the concentration gradient constant—further confirming that electromigration and ion diffusion work additively to enhance electroconvection.

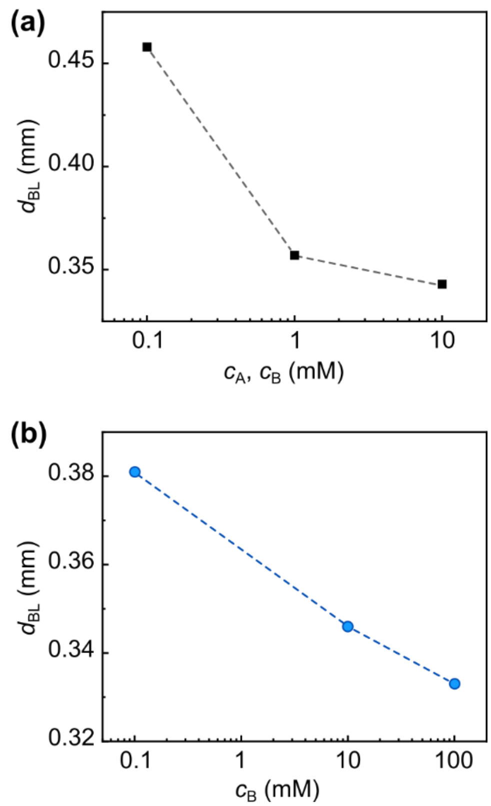

Figure 5. Maximum thickness of the depletion boundary layer as a function of (a) concentration ($c_A = c_B$) and (b) concentration gradient. A constant flow rate of Q = 0.2 mL/h was used for all experiments. A constant concentration of c_A = 1 mM was used for (b).

While the measured d_{BL} values shown in Figures 4b and 4d vary depending on i) the mutual directions of the concentration gradient and the electric field and ii) the concentration gradient, those are relatively insensitive in comparison to the measured currents as shown in Figure 4a and 4c. A simple scaling analysis can provide physical insights on the observation. The scaling of d_{EC} can be obtained from a momentum balance between pressure gradient (responsible for tangential flow parallel to the membrane) and electrical body force (responsible for vortex flows) due to an external electric field),[34] conceptually analogous to the boundary layer theory.[46] This indicates that $d_{EC}/w \sim (\varphi^2/U)^{1/3}$ where w is the channel width, φ is an applied potential and U is an average fluid velocity, implying that it would be relatively insensitive to the mutual directions of the concentration gradient and the electric field. On the other hand, ion transport (or ion flux) can be described by Nernst-Planck equation, a conservation of ion flux, that includes contributions from advection, diffusion, and electromigration. A scaling analysis for Nernst-Planck equation[47] shows that three contributions would be comparable because ion Peclét number that indicates the order of advective contribution is $O(1)$, considering that typical values of viscosity of solution (~ 1cP), dielectric constant of the solution (~ 80), and ion mobility (~ 10^{-9} m^2/sec) at room temperature. Note that ion Peclét number is defined as $\varepsilon\varepsilon_0 kT/e^2\mu\omega$ where ε is the dielectric constant of solution, ε_0 is the vacuum permittivity, k is the Boltzmann constant, T is the temperature, e is the element charge, μ is the viscosity of solution, and ω is ion mobility. This suggests that the additional diffusional contribution from the concentration gradient cannot be negligible for ion transport. In fact, even for the opposed cases, the ion current with the larger concentration gradient (i.e., 10 mM/1mM) shown in the blue curve of Figure 4c is an order of magnitude larger than that with the smaller concentration gradient (i.e., 1 mM/0.1mM) shown in the blue curve of Figure 4a. Similarly, the aligned case with the smaller concentration gradient demonstrates a relatively smaller deviation in the current from the opposed case shown in Figure 4a (red vs. blue curves), compared to the case with the larger concentration gradient shown in Figure 4c (red vs. blue curves).

To understand the influence of flow rate, we investigated its effects on electroconvection with and without concentration gradients. Using the same microfluidic device with the same concentration gradient conditions (c_A = 1 mM and c_B = 10 mM), we performed LSV experiments at different flow rates Q. The largest electroconvective vortices were observed at the largest applied voltage closer to the end of the flow channel (similar to Figure 3b). Figure 6a shows frames with the maximum thickness of the depletion boundary layer d_{BL} at different flow rates from 0 to

1 mL/h. The largest $d_{BL} = 0.48$ mm was obtained without flow ($Q = 0$), and the d_{BL} value decreased to 0.15 mm at Q = 1.0 mL/h. Clearly, an increasing flow rate yielded a smaller d_{BL} values, suggesting tangential fluid flow suppressed electroconvection. To quantitatively characterize this suppression, we performed systematic measurements of d_{BL} in the absence of concentration gradients ($c_A = c_B = 0.1$, 1, and 10 mM) and with concentration gradients (c_A = 1 mM =const., c_B = 0.1, 1, and 10 mM). The plots in Figures 6b,c both show that d_{BL} decreases with an increasing flow rate both in the absence and presence of concentration gradients. Given the fluctuations for different concentration conditions, for a given flow rate, the d_{BL} values appear to be within a similar range for the presence and absence of concentration gradient. Our finding of flow-suppressed electroconvection are in agreement with a previously reported suppression of electroconvection in dendrite growth on Cu and Zn electrodes.[48]

Furthermore, the maximum measured decrease in d_{BL} is 0.41 mm in Figure 6c, from 0.48 to 0.07 mm with the employed flow rate ranging from 0 to 1 mL/h. In comparison, varying the concentration and concentration gradient by several orders of magnitude only resulted in small deceases in d_{BL}, 0.12 mm for Figure 5a and 0.05 mm for Figure 5b. These results suggest that the flow rate has a more significant direct influence on the thickness of the depletion boundary layer compared to the presence and the strength of a concentration gradient. We note that the direction of these vectorial parameters could explain this difference, i.e., the growth direction of electroconvective vortices is normal with the fluid flow direction, but parallel to the direction of concentration gradient. Furthermore, plotting the dimensionless electroconvection sizes d_{EC}/w as a function of $(\phi^2/U)^{1/3}$ shows good agreement between our data and the theoretical scaling law for conditions with zero and negative concentration gradients (Figure S2). Note that our electroconvection experiments explored a narrower parameter space (flow rates 0-1mL/h, applied voltages 5.9 to 9.6 V) compared to the original study by Kwak et al. that introduced the scaling law.[34] The weaker correlation for the condition with a positive concentration gradient could be related to the narrow parameter windows. Nonetheless, our data with d_{EC}/w in the range of 0.05 to 0.25 and the scaling factor in the range 30 to 60 are in good agreement with those reported by Kwak et al.[34] indicating the applicability of the scaling law that governs the thickness of electroconvective vortex under shear flow even in the presence of concentration gradients.

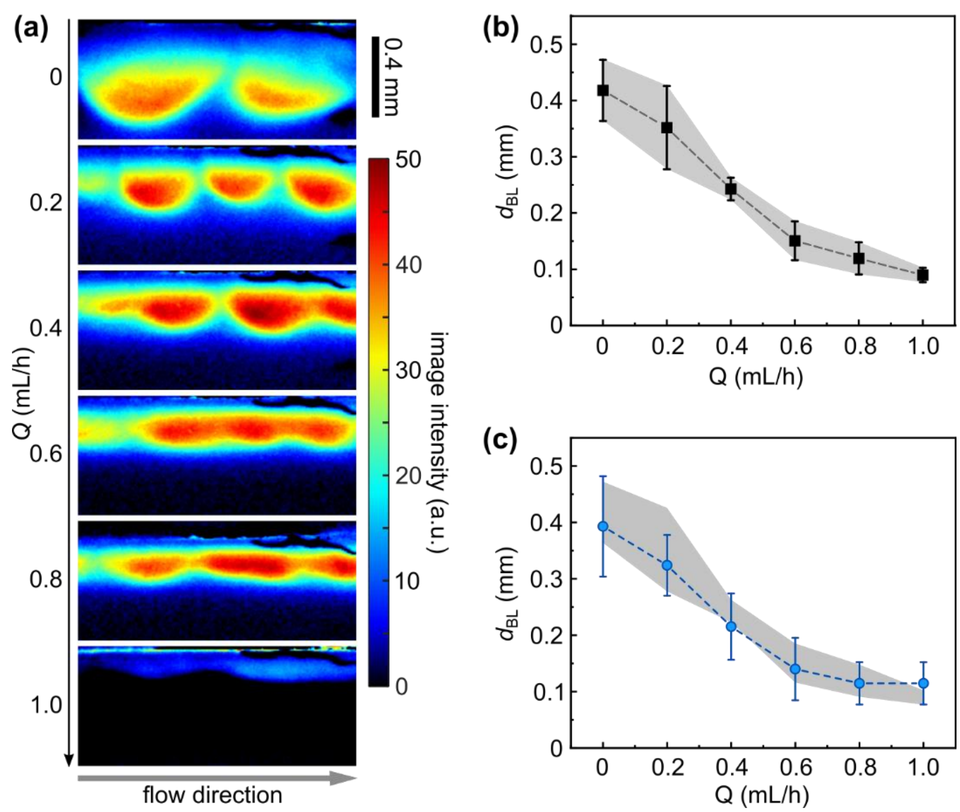

Figure 6. (a) False-colored images at different flow rates with c_A = 1 mM and c_B = 10 mM. Maximum thickness of the depletion boundary layer d_{BL} as a function of flow rate (b) without and (c) with concentration gradients. The gray area in (c) is obtained from the error bars in (b) for comparison purposes.

The linear sweep rate in our LSV experiments was 100 mV/s, so the experimental time during which electroconvection was observable was typically very short, approximately 40 s from the onset of electroconvection to the end of the experiment. To overcome the limitation of short observation time windows, we used chronoamperometry (CA) to study electroconvection in the microfluidic device. In a typical CA experiment, a select voltage was applied to the electrodes and held for a certain period of time. Figure 7a shows consecutive frames of electroconvection at the membrane surface at 7 V without concentration gradients ($c_A = c_B = 1$ mM). The vortex patterns moved along the flow direction, but their sizes remained nearly the same for about 60 s. To show the steadiness of the electroconvection under CA without a concentration gradient, we obtained a color profile from each frame by averaging the image intensity along the flow direction. Several examples were shown on the right panel (i-v) of Figure 7a. Each profile is 1 pixel wide and spans 180 pixels (0.4 mm). Then these color profiles were stacked chronologically in the time-space plot in Figure 7b. The plateau-like feature indicates a nearly constant d_{BL} value of 0.25 mm, which is marked by the dashed line.

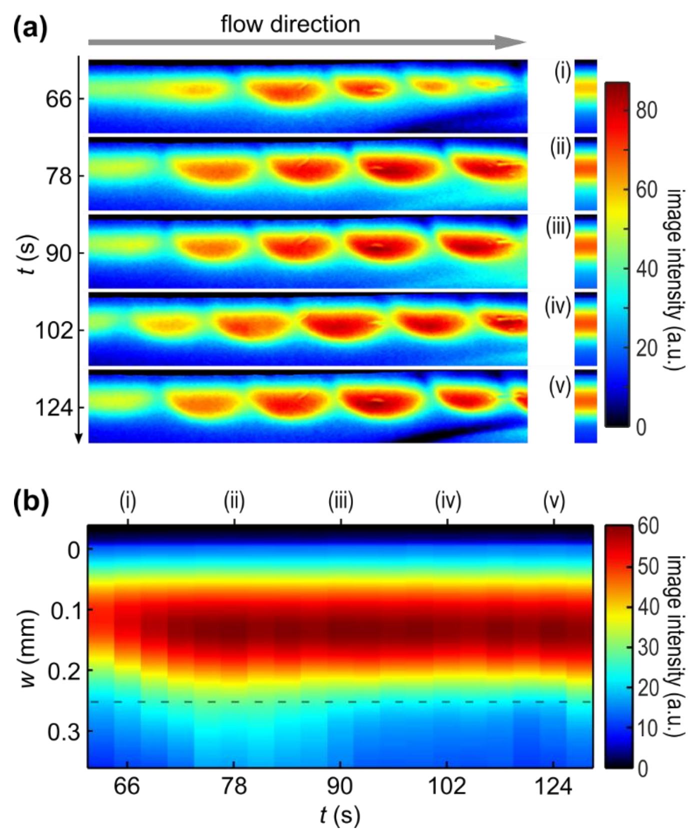

Figure 7. (a) False-colored image frames showing electroconvection at a constant voltage without concentration gradients. (i-v) are averaged color profiles from each frame. (b) Time-space plot of electroconvection at 7 V without concentration gradients. Experimental condition: $c_A = c_B = 1$ mM, $Q = 0.2$ mL/h.

Furthermore, we systematically compared the electroconvection without (Figures 8a-c) and with (Figures 8d-e) concentration gradients using CA and under a series of constant applied voltage values. Without concentration gradients ($c_A = c_B = 0.1$ mM), the applied voltages were held at 4, 5, 6, and 7 V for 20 s each (Figure 8a). These selected voltage values were close to the onset of electroconvection as generally at higher voltages strong electroconvection co-occurred with bubble formation reducing the viable observation window. The measured current increased with increase in voltage and then slowly decayed (Figure 8b). The decaying current suggests an increase in electrical resistivity of the system, possibly due to redox reactions leading to gaseous byproducts that form bubbles at the electrode surface disrupting electrical contact in the device. The other key factor responsible for current decay is the reduced ion transport across the membrane due to the formation of an ion depletion layer. The time-space plot in Figure 8c shows temporal evolution of the electroconvection at constant applied voltages. The plot was constructed by stacking averaged color profiles chronologically with red and blue colors indicating large and small decreases in image (fluorescence) intensity. We observed a large decrease in fluorescence intensity especially at the core of the electroconvective vortices at higher voltages (deep red colors at w = 0.03-0.1 mm). In addition, we quantitatively characterized the intensity of electroconvection by measuring the d_{BL} values from the time-space plot. The red dotted curve in Figure 8d marks the edge of the electroconvective vortices at each time point. Our data shows that d_{BL} gradually increased each time when the voltage was raised and then kept nearly constant around 0.55, 0.17, 0.23, and 0.26 mm at 4, 5, 6, and 7 V, respectively. The fluctuation of d_{BL} was mainly caused by the large vortices moving out of the view window. As previously experimentally observed[34] and theoretically predicted,[39] the size of the vortices is larger farthest from the inlet.

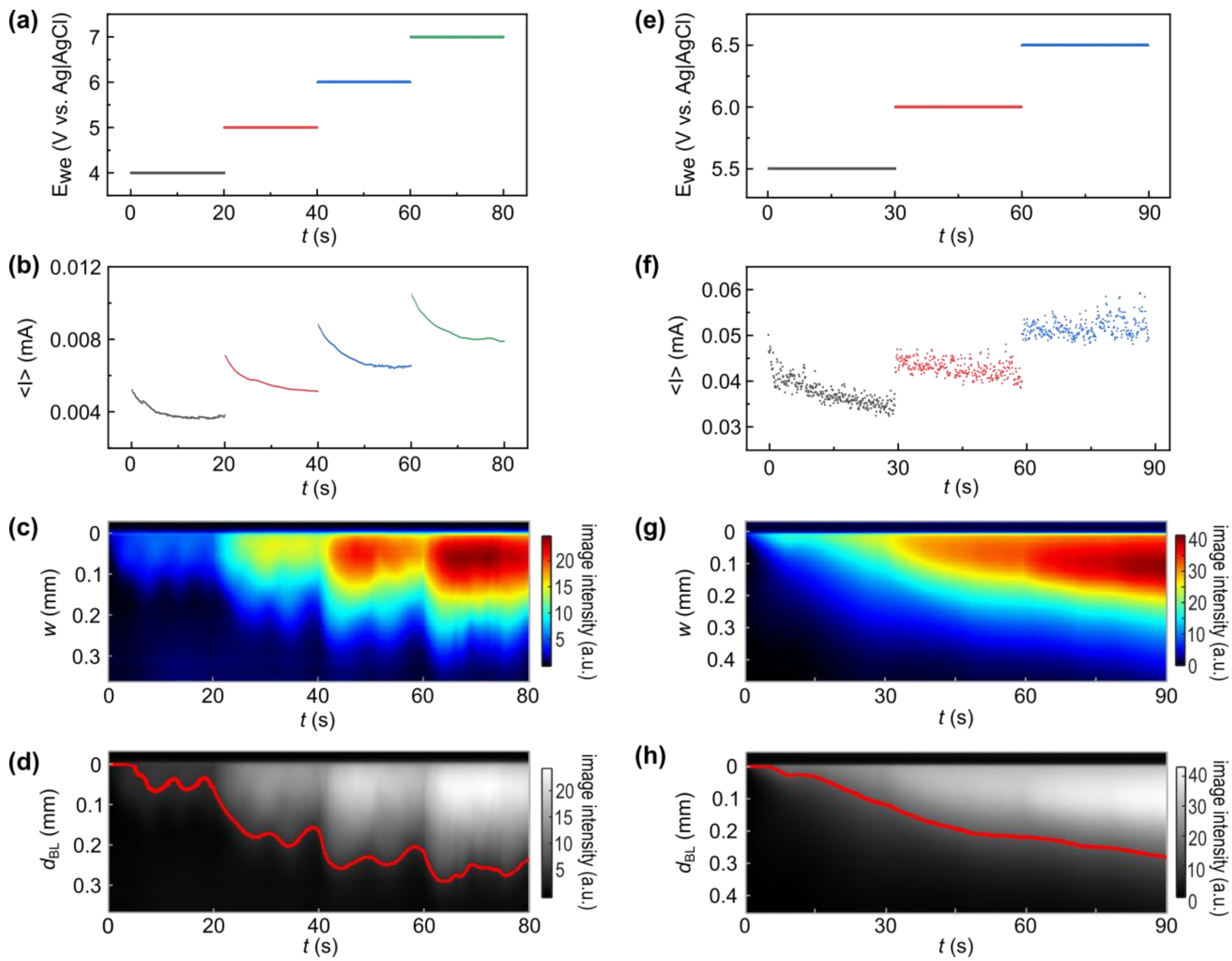

Figure 8. Chronoamperometry and spatiotemporal dynamics without (a-d, left column) and with (e-h, right column) concentration gradients. (a, e) Constant voltages were hold for 20 s (a) and 30 s (e). (b, f) Measured current. (c, g) Time-space plots. (d, h) d_{BL} as a function of time. Experimental conditions: $c_A = c_B = 0.1$ mM (a-d); $c_A = 10$ mM, $c_B = 1$ mM (e-h); $Q = 0.2$ mL/h for both.

For the experiments with a concentration gradient ($c_A = 10$ mM, $c_B = 1$ mM), we held the applied voltages at 5.5, 6, and 6.5 V for 30 s each (Figure 8e). The measured currents in Figure 8f showed a similar decaying trend but with larger variations compared to the values without concentration gradients. We also observed a continuous and gradual increase in the size and intensity of electroconvection according to the time-space plot in Figure 8g. This result differs from the stepwise and plateaus-like features that we observed in the absence of a concentration gradient. The smooth increase in d_{BL} (Figure 8h) is possibly related to persistent ion diffusion driven by the concentration gradient. Note that the black bars on the top of Figures 8c,d,g, and h are from the Nafion membrane where the image intensity did not change.

CONCLUSION

We designed and developed a microfluidics device to investigate the influence of ion concentration gradients across a cation exchange membrane (Nafion N115). Our device closely mimicked an electrodialysis configuration with electric field normal to the direction of fluid flow. We used this system to study the onset and nature of electroconvection both when the concentration gradients are aligned with and opposed to the applied electric field. Experiments characterizing the depletion boundary layer with and without concentration gradients found that electromigration and ion diffusion work additively to enhance electroconvection. The influence of flow rates was significant and the largest electroconvective vortices were observed at the end of the flow channels, which is consistent with prior studies. However, the measurable influence of concentration gradients as a function of flow rate was negligible. Most importantly, our results show that electroconvection is most pronounced when the electric field is opposed to the direction of the concentration gradient, and the direction of the electric field alone determines which surface of the membrane electroconvection occurs at. These findings offer direct insights into how ion separation efficiencies of electric field driven, membrane-based systems such as electrodialysis can be improved.

Notes

The authors declare no competing financial interest.

ACKNOWLEDGMENT

This work was supported by the Laboratory Directed Research and Development Program (LDRD) at Pacific Northwest National Laboratory (PNNL). PNNL is a multiprogram national laboratory operated for DOE by Battelle under contract DE-AC05-76RLO1830. Part of this work was conducted at the Molecular Analysis Facility, a National Nanotechnology Coordinated Infrastructure (NNCI) site at the University of Washington with partial support from the National Science Foundation via awards NNCI-2025489 and NNCI-1542101. We thank E. Allen for the assistance with the experimental setup.

REFERENCES

(1) Greve, P.; Kahil, T.; Mochizuki, J.; Schinko, T.; Satoh, Y.; Burek, P.; Fischer, G.; Tramberend, S.; Burtscher, R.; Langan, S.; Wada, Y., Global Assessment of Water Challenges under Uncertainty in Water Scarcity Projections. *Nat. Sustain.* **2018,** *1* (9), 486-494.

(2) Mauter, M. S.; Fiske, P. S., Desalination for a Circular Water Economy. *Energy Environ. Sci.* **2020,** *13* (10), 3180-3184.

(3) Strathmann, H., Electrodialysis, a Mature Technology with a Multitude of New Applications. *Desalination* **2010,** *264* (3), 268-288.

(4) Garcia-Vasquez, W.; Dammak, L.; Larchet, C.; Nikonenko, V.; Pismenskaya, N.; Grande, D., Evolution of Anion-Exchange Membrane Properties in a Full Scale Electrodialysis Stack. *J. Membr. Sci.* **2013,** *446*, 255-265.

(5) Bian, D. W.; Watson, S. M.; Wright, N. C.; Shah, S. R.; Buonassisi, T.; Ramanujan, D.; Peters, I. M.; Winter, A. G., Optimization and Design of a Low-Cost, Village-Scale, Photovoltaic-Powered, Electrodialysis Reversal Desalination System for Rural India. *Desalination* **2019,** *452*, 265-278.

(6) Zabolotsky, V. I.; Nikonenko, V. V.; Pismenskaya, N. D.; Laktionov, E. V.; Urtenov, M. K.; Strathmann, H.; Wessling, M.; Koops, G. H., Coupled Transport Phenomena in Overlimiting Current Electrodialysis. *Sep. Purif. Technol.* **1998,** *14* (1), 255-267.

(7) Mishchuk, N. A., Electro-Osmosis of the Second Kind near the Heterogeneous Ion-Exchange Membrane. *Colloids Surf., A* **1998,** *140* (1), 75-89.

(8) Nikonenko, V. V.; Kovalenko, A. V.; Urtenov, M. K.; Pismenskaya, N. D.; Han, J.; Sistat, P.; Pourcelly, G., Desalination at Overlimiting Currents: State-of-the-Art and Perspectives. *Desalination* **2014,** *342*, 85-106.

(9) Mani, A.; Wang, K. M., Electroconvection near Electrochemical Interfaces: Experiments, Modeling, and Computation. *Annu. Rev. Fluid Mech.* **2020,** *52* (1), 509-529.

(10) Uzdenova, A. M.; Kovalenko, A. V.; Urtenov, M. K.; Nikonenko, V. V., Effect of Electroconvection During Pulsed Electric Field Electrodialysis. Numerical Experiments. *Electrochem. Commun.* **2015,** *51*, 1-5.

(11) Rubinstein, I.; Staude, E.; Kedem, O., Role of the Membrane Surface in Concentration Polarization at Ion-Exchange Membrane. *Desalination* **1988,** *69* (2), 101-114.

(12) Rubinstein, I.; Zaltzman, B., Electro-Osmotically Induced Convection at a Permselective Membrane. *Phys. Rev. E* **2000,** *62* (2), 2238-2251.

(13) Zaltzman, B.; Rubinstein, I., Electro-Osmotic Slip and Electroconvective Instability. *J. Fluid Mech.* **2007,** *579*, 173-226.

(14) Rubinstein, I.; Zaltzman, B., Equilibrium Electroconvective Instability. *Phys. Rev. Lett.* **2015,** *114* (11), 114502.

(15) Abu-Rjal, R.; Rubinstein, I.; Zaltzman, B., Driving Factors of Electro-Convective Instability in Concentration Polarization. *Phys. Rev. Fluids* **2016,** *1* (2), 023601.

(16) Vasil'eva, V. I.; Shaposhnik, V. A.; Grigorchuk, O. V.; Petrunya, I. P., The Membrane–Solution Interface under High-Performance Current Regimes of Electrodialysis by Means of Laser Interferometry. *Desalination* **2006,** *192* (1), 408-414.

(17) Zabolotsky, V. I.; Novak, L.; Kovalenko, A. V.; Nikonenko, V. V.; Urtenov, M. H.; Lebedev, K. A.; But, A. Y., Electroconvection in Systems with Heterogeneous Ion-Exchange Membranes. *Pet. Chem.* **2017,** *57* (9), 779-789.

(18) Titorova, V. D.; Mareev, S. A.; Gorobchenko, A. D.; Gil, V. V.; Nikonenko, V. V.; Sabbatovskii, K. G.; Pismenskaya, N. D., Effect of Current-Induced Coion Transfer on the Shape of Chronopotentiograms of Cation-Exchange Membranes. *J. Membr. Sci.* **2021,** *624*, 119036.

(19) Rybalkina, O. A.; Sharafan, M. V.; Nikonenko, V. V.; Pismenskaya, N. D., Two Mechanisms of H^+/OH^- Ion Generation in Anion-Exchange Membrane Systems with Polybasic Acid Salt Solutions. *J. Membr. Sci.* **2022,** *651*, 120449.

(20) Titorova, V. D.; Moroz, I. A.; Mareev, S. A.; Pismenskaya, N. D.; Sabbatovskii, K. G.; Wang, Y.; Xu, T.; Nikonenko, V. V., How Bulk and Surface Properties of Sulfonated Cation-Exchange Membranes Response to Their Exposure to Electric Current During Electrodialysis of a Ca^{2+} Containing Solution. *J. Membr. Sci.* **2022,** *644*, 120149.

(21) Akberova, E. M.; Vasil'eva, V. I., Effect of the Resin Content in Cation-Exchange Membranes on Development of Electroconvection. *Electrochem. Commun.* **2020,** *111*, 106659.

(22) Rubinstein, S. M.; Manukyan, G.; Staicu, A.; Rubinstein, I.; Zaltzman, B.; Lammertink, R. G. H.; Mugele, F.; Wessling, M., Direct Observation of a Nonequilibrium Electro-Osmotic Instability. *Phys. Rev. Lett.* **2008,** *101* (23), 236101.

(23) Yossifon, G.; Chang, H.-C., Selection of Nonequilibrium Overlimiting Currents: Universal Depletion Layer Formation Dynamics and Vortex Instability. *Phys. Rev. Lett.* **2008,** *101* (25), 254501.

(24) Kwak, R.; Guan, G.; Peng, W. K.; Han, J., Microscale Electrodialysis: Concentration Profiling and Vortex Visualization. *Desalination* **2013,** *308*, 138-146.

(25) de Valença, J. C.; Wagterveld, R. M.; Lammertink, R. G. H.; Tsai, P. A., Dynamics of Microvortices Induced by Ion Concentration Polarization. *Phys. Rev. E* **2015,** *92* (3), 031003.

(26) Pande, N.; Wood, J. A.; Mul, G.; Lohse, D.; Mei, B. T.; Krug, D., Electroconvective Instability in Water Electrolysis: An Evaluation of Electroconvective Patterns and Their Onset Features. *Phys. Rev. Appl.* **2021,** *16* (3), 034021.

(27) Warren, A.; Sharma, A.; Zhang, D.; Li, G.; Archer, L. A., Structure and Dynamics of Electric-Field-Driven Convective Flows at the Interface between Liquid Electrolytes and Ion-Selective Membranes. *Langmuir* **2021,** *37* (19), 5895-5901.

(28) Sharma, A.; Mukherjee, A.; Warren, A.; Jin, S.; Li, G.; Koch, D. L.; Archer, L. A., Electroconvective Flow in Liquid Electrolytes Containing Oligomer Additives. *Langmuir* **2023,** *39* (1), 92-100.

(29) Nikonenko, V. V.; Vasil'eva, V. I.; Akberova, E. M.; Uzdenova, A. M.; Urtenov, M. K.; Kovalenko, A. V.; Pismenskaya, N. P.; Mareev, S. A.; Pourcelly, G., Competition between Diffusion and Electroconvection at an Ion-Selective Surface in Intensive Current Regimes. *Adv. Colloid Interface Sci.* **2016,** *235*, 233-246.

(30) de Valença, J.; Jõgi, M.; Wagterveld, R. M.; Karatay, E.; Wood, J. A.; Lammertink, R. G. H., Confined Electroconvective Vortices at Structured Ion Exchange Membranes. *Langmuir* **2018,** *34* (7), 2455-2463.

(31) Stockmeier, F.; Stüwe, L.; Kneppeck, C.; Musholt, S.; Albert, K.; Linkhorst, J.; Wessling, M., On the Interaction of Electroconvection at a Membrane Interface with the Bulk Flow in a Spacer-Filled Feed Channel. *J. Membr. Sci.* **2023,** *678*, 121589.

(32) Seo, M.; Kim, W.; Lee, H.; Kim, S. J., Non-Negligible Effects of Reinforcing Structures inside Ion Exchange Membrane on Stabilization of Electroconvective Vortices. *Desalination* **2022,** *538*, 115902.

(33) Stockmeier, F.; Schatz, M.; Habermann, M.; Linkhorst, J.; Mani, A.; Wessling, M., Direct 3D Observation and Unraveling of Electroconvection Phenomena During Concentration Polarization at Ion-Exchange Membranes. *J. Membr. Sci.* **2021,** *640*, 119846.

(34) Kwak, R.; Pham, V. S.; Lim, K. M.; Han, J., Shear Flow of an Electrically Charged Fluid by Ion Concentration Polarization: Scaling Laws for Electroconvective Vortices. *Phys. Rev. Lett.* **2013,** *110* (11), 114501.

(35) Kang, S.; Kwak, R., Pattern Formation of Three-Dimensional Electroconvection on a Charge Selective Surface. *Phys. Rev. Lett.* **2020,** *124* (15), 154502.

(36) Campione, A.; Gurreri, L.; Ciofalo, M.; Micale, G.; Tamburini, A.; Cipollina, A., Electrodialysis for Water Desalination: A Critical Assessment of Recent Developments on Process Fundamentals, Models and Applications. *Desalination* **2018,** *434*, 121-160.

(37) Chang, H.-K.; Choi, E.; Park, J., Paper-Based Energy Harvesting from Salinity Gradients. *Lab Chip* **2016,** *16* (4), 700-708.

(38) Wang, Q.; Steinbock, O., Flow-Assisted Self-Organization of Hybrid Membranes. *Chem. Eur. J.* **2019,** *25* (44), 10427-10432.

(39) Urtenov, M. K.; Uzdenova, A. M.; Kovalenko, A. V.; Nikonenko, V. V.; Pismenskaya, N. D.; Vasil'eva, V. I.; Sistat, P.; Pourcelly, G., Basic Mathematical Model of Overlimiting

Transfer Enhanced by Electroconvection in Flow-through Electrodialysis Membrane Cells. *J. Membr. Sci.* **2013,** *447*, 190-202.

(40) Peers, A., Membrane Phenomena. *Discuss. Faraday Soc* **1956,** *21*, 124-125.

(41) Belova, E. I.; Lopatkova, G. Y.; Pismenskaya, N. D.; Nikonenko, V. V.; Larchet, C.; Pourcelly, G., Effect of Anion-Exchange Membrane Surface Properties on Mechanisms of Overlimiting Mass Transfer. *J. Phys. Chem. B* **2006,** *110* (27), 13458-13469.

(42) Huo, P.; Xu, B.; Gu, Z.; Su, M.; Rubinstein, S. M.; Deng, D., Observation of Remote Electroconvection and Inert-Cation Concentration Valley within Supporting Electrolytes in a Microfluidic-Based Electrochemical Device. *Small* **2022,** *18* (18), 2108037.

(43) Kumar, P.; Rubinstein, S. M.; Rubinstein, I.; Zaltzman, B., Mechanisms of Hydrodynamic Instability in Concentration Polarization. *Phys. Rev. Res.* **2020,** *2* (3), 033365.

(44) Belloň, T.; Polezhaev, P.; Vobecká, L.; Svoboda, M.; Slouka, Z., Experimental Observation of Phenomena Developing on Ion-Exchange Systems During Current-Voltage Curve Measurement. *J. Membr. Sci.* **2019,** *572*, 607-618.

(45) Mishchuk, N. A., Concentration Polarization of Interface and Non-Linear Electrokinetic Phenomena. *Adv. Colloid Interface Sci.* **2010,** *160* (1), 16-39.

(46) R. Byron Bird; Warren E. Stewart; Lightfoot, E. N., *Transport Phenomena*. 2nd Edition ed.; J. Wiley: New York, 2007.

(47) Russel, W. B.; Russel, W.; Saville, D. A.; Schowalter, W. R., *Colloidal Dispersions*. Cambridge university press: 1991.

(48) Ma, M. C.; Li, G.; Chen, X.; Archer, L. A.; Wan, J., Suppression of Dendrite Growth by Cross-Flow in Microfluidics. *Sci. Adv.* **2021,** *7* (8), eabf6941.

Table of Contents Graphic